



This is a repository copy of *Photo-Induced Cytotoxicity and Anti-Metastatic Activity of Ruthenium(II)-Polypyridyl Complexes Functionalized with Tyrosine or Tryptophan*.

White Rose Research Online URL for this paper:
<http://eprints.whiterose.ac.uk/115262/>

Version: Accepted Version

Article:

Ramu, V., Aute, S., Taye, N. et al. (7 more authors) (2017) Photo-Induced Cytotoxicity and Anti-Metastatic Activity of Ruthenium(II)-Polypyridyl Complexes Functionalized with Tyrosine or Tryptophan. *Dalton Transactions*, 46. pp. 6634-6644. ISSN 1477-9226

<https://doi.org/10.1039/C7DT00670E>

Reuse

Items deposited in White Rose Research Online are protected by copyright, with all rights reserved unless indicated otherwise. They may be downloaded and/or printed for private study, or other acts as permitted by national copyright laws. The publisher or other rights holders may allow further reproduction and re-use of the full text version. This is indicated by the licence information on the White Rose Research Online record for the item.

Takedown

If you consider content in White Rose Research Online to be in breach of UK law, please notify us by emailing eprints@whiterose.ac.uk including the URL of the record and the reason for the withdrawal request.



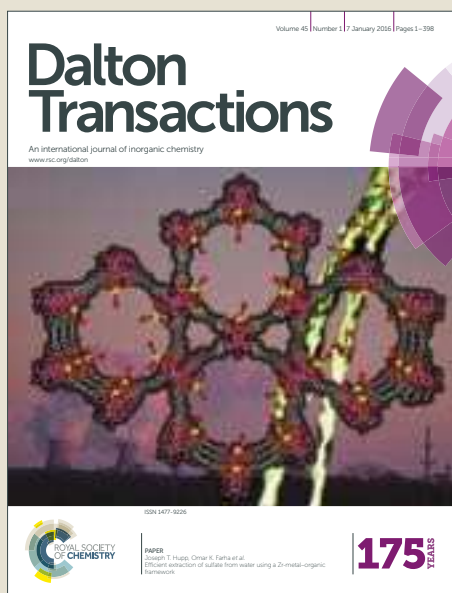
eprints@whiterose.ac.uk
<https://eprints.whiterose.ac.uk/>

Dalton Transactions

Accepted Manuscript



This article can be cited before page numbers have been issued, to do this please use: V. Ramu, S. Aute, N. Taye, R. Guha, M. G. Walker, D. G. Mogare, A. Parulekar, J. Thomas, S. Chattopadhyay and A. Das, *Dalton Trans.*, 2017, DOI: 10.1039/C7DT00670E.



This is an Accepted Manuscript, which has been through the Royal Society of Chemistry peer review process and has been accepted for publication.

Accepted Manuscripts are published online shortly after acceptance, before technical editing, formatting and proof reading. Using this free service, authors can make their results available to the community, in citable form, before we publish the edited article. We will replace this Accepted Manuscript with the edited and formatted Advance Article as soon as it is available.

You can find more information about Accepted Manuscripts in the [author guidelines](#).

Please note that technical editing may introduce minor changes to the text and/or graphics, which may alter content. The journal's standard [Terms & Conditions](#) and the ethical guidelines, outlined in our [author and reviewer resource centre](#), still apply. In no event shall the Royal Society of Chemistry be held responsible for any errors or omissions in this Accepted Manuscript or any consequences arising from the use of any information it contains.



Journal Name

ARTICLE

Photo-Induced Cytotoxicity and Anti-Metastatic Activity of Ruthenium(II)-Polypyridyl Complexes Functionalized with Tyrosine or Tryptophan

Received 00th January 20xx,
Accepted 00th January 20xx

DOI: 10.1039/x0xx00000x

www.rsc.org/

Vadde Ramu,^a Sunil Aute,^a Nandaraj Taye,^b Rweetuparna Guha,^a Michael G. Walker,^c Devaraj Mogare,^b Apoorva Parulekar,^b Jim A Thomas*,^c Samit Chattopadhyay*^{b,d} and Amitava Das*^{a,e}

The synergistic effect of oxygen, light, and photosensitizer (PS) has found applications in medicine for the treatment of cancer through photodynamic therapy (PDT). Induction of apoptosis to cancerous cells will prevent tumor metastasis that spreads cancer cells to the neighboring organs/tissues. Herein, we report the two apoptotic Ru(II)-polypyridyl complexes that are functionalized with pendent amino acid moieties tyrosine (1) and tryptophan (2), respectively. These two water soluble complexes were found to interact strongly ($K_a^1 = (1.18 \pm 0.28)10^5 \text{ M}^{-1}$ and $K_a^2 = (1.57 \pm 0.77)10^5 \text{ M}^{-1}$) with CT-DNA. Isothermal titration calorimetry (ITC) studies revealed that these complexes bind to CT-DNA through an entropically driven process. Both the complexes showed photo-induced cytotoxicity and exhibits apoptotic activity under photo-irradiation conditions. The comet assay indicated that these complexes can damage cellular DNA, which was attributed to the significant buildup of $^1\text{O}_2$ level even on irradiation with low intensity light (10 J/cm^2 , $\lambda_{\text{Range}} 450 - 480 \text{ nm}$). This photoinduced DNA damage and apoptosis in A549 cells were induced by reactive oxygen species (ROS) and occurred through up-regulation of apoptotic marker caspase-3. Control experiments under the dark condition revealed an insignificant cytotoxicity towards these cells for two photosensitive molecules.

1. Introduction

According to the World Health Organization (WHO), cancer is the leading cause of death all around the world.¹ One of the defining features of cancer is the rapid creation of abnormal cells that grow beyond their usual boundaries, which can then invade adjoining parts of the body and spread to other organs, the latter process is known as metathesis. Photodynamic therapy (PDT) is non-invasive and one of the most extensively used techniques for dermatological diseases and various types of cancers, which could be used to control and selectively treat solid tumors.²⁻⁴ The main advantage of PDT over traditional therapies such as surgery, radiation and chemotherapy are that PDT produces fewer side effects. PDT requires a photosensitizer or photosensitizing agent (PS) that is therapeutically activated in the presence of light.⁵ Ideally, the PDT reagent should not show any such activity in the dark. The activity of such PDT reagents mainly depends on the efficiency

of the PS molecule or fragment in generating long-lived excited state. On excitation of the PS moiety at an appropriate wavelength, energy or electron transfer process eventually lead to the generation of reactive oxygen species (ROS) like superoxide anion ($\text{O}_2^{\cdot-}$), hydroxyl radical (HO^{\cdot}), hydrogen peroxide and singlet oxygen ($^1\text{O}_2$). Such ROS species are known to be cytotoxic to living cells and can be judiciously utilized for targeted singlet oxygen chemotherapy. Tumor metastasis is a multistep biological process that allows cancer cells to move away from the primary tumor, survive in the circulation system, locate in distal sites and grow.⁶ Thus, more recently it has been argued that effective treatment for cancer largely depends on therapeutics that not only induces cell cycle arrest but also possess anti-metastatic activity. Commercially available PS agents such as hematoporphyrins and its derivatives (HpD) generally suffer from drawbacks such as low solubility in aqueous solutions and weak absorption band at 630 nm. This necessitates the use of high light doses of $100\text{--}200 \text{ J/cm}^2$ to achieve the desired control of tumor growth. Also, common PDT drugs like Porfimer sodium can cause severe side effects, as they are retained in the body for about 4 months and results in skin photosensitivity.⁷ More recently, the European Union has approved the use of meso-tetra hydroxyphenyl chlorin (mTHPC) as a PS for PDT application.⁵⁻⁷ However, these agents suffer from poor stability in physiological conditions and also photobleach on photo-irradiation.^{5,8} These drawbacks limit the use of these reagents for PDT applications; thus, there is a definite scope for

^a Organic Chemistry Division, CSIR-National Chemical Laboratory, Pune, 411008, India

^b Chromatin and Disease Biology Laboratory, National Centre for Cell Science, Pune, 411007, India

^c Department of Chemistry, University of Sheffield, Sheffield, UK. E-mail: james.thomas@sheffield.ac.uk

^d Indian Institute of Chemical Biology, Kolkata: 700 032, West Bengal, India; E-mail: samit@iicb.res.in

^e CSIR-Central Salt and Marine Chemicals Research Institute, Bhavnagar, 364002, Gujarat, India E-mail: a.das@csmcric.res.in

†Electronic Supplementary Information (ESI) See DOI: 10.1039/x0xx00000x

ARTICLE

Journal Name

developing appropriate reagents that can overcome foresaid disadvantages. After the successful entry of ruthenium-based drugs (NAMI-A and KP1019) into human clinical trials, there is a burgeoning interest in developing Ru(II)-based novel anticancer drugs with new and improved function.^{8,9} The possibility of achieving high solubility by choosing appropriate counter anions or through appropriate functionalization of the coordinated ligands has led to the design of new Ru(II)-polypyridyl complexes for use of anti-cancer and anti-metastatic drugs.^{10,11} These complexes are attractive choices for use as photodynamic therapeutic reagents and they also possess visible light excitation, reasonably long-lived triplet excited states, and higher stability towards photobleaching.⁷ Recent reports suggested that the conjugation of biologically relevant molecules to the Ru(II)-polypyridyl complexes can improve cellular internalization.^{12,13} Ru(II)-polypyridyl complexes with appropriately functionalized bpy derivative can enhance lipophilicity and can lead to more efficient internalization.^{14–17} Herein, we investigated the use of two Ru(II)-polypyridyl based reagents with pendant tyrosine or tryptophan moiety as efficient PDT reagents. Photo-induced cytotoxicity, anti-metastatic property, cellular uptake and ROS-mediated DNA cleaving pathways for these two complexes (**1** and **2**) are described. Significantly it has been found that these systems are active as PDT sensitizers at light doses as low as 10 J/cm².

2. Results and discussion

Synthesis of **1** and **2** was achieved by following previously reported literature procedures.^{18,19} Both complexes were characterized using a range of spectroscopic and analytical techniques. All these spectroscopic data, as well as the results of elemental analysis, confirm the desired purity for both complexes utilized in our studies (fig. S8-11). The photophysical properties of these two complexes are well established and this is the primary reason for choosing them for our studies. Tyrosine is a non-essential amino acid that plays a crucial role in the protein synthesis and acts as a receiver of phosphate groups in biological systems that are transferred by way of protein kinases (so-called receptor tyrosine kinases).²⁰ Also, it is involved in the mechanism of photosynthetic oxidation of water into molecular oxygen in photosystem II (PSII).²¹ The tryptophan moiety that is utilized in designing complex **2** is an essential amino acid that cannot be synthesized by higher organisms. Tyrosine and tryptophan derivatives are known to readily cross the blood–brain barrier and facilitate cellular internalization.²² On the other hand, Ru(II)-polypyridyl complexes are known to generate reactive oxygen species (ROS) up on irradiation into their MLCT band in the visible region of the spectrum.^{23–26} As outlined above, such ROS species damage biomolecules and are therefore cytotoxic to living cells.^{27–29} Since these two complexes are functionalized with amino acid moieties to enhance cellular internalization and possess well-defined photophysical/physicochemical properties, their capability to

photo-induced damage to the DNA and function as cytotoxic agents was investigated.

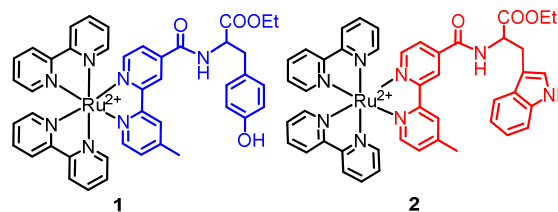


Figure 1. Chemical structures of complex **1** and **2**.

DNA binding studies.

Water soluble complexes **1** and **2** with Cl[−] as counter anion were obtained via anion metathesis. The interactions of complexes **1** and **2** with CT-DNA were investigated using UV-Visible and fluorescence spectroscopy. The addition of small aliquots of CT-DNA to the buffer solution containing **1** or **2** led to an appreciable hypochromic shift in the $\pi \rightarrow \pi^*$ (290 nm) based transition, while slight change was registered for the MLCT (450 nm)-based absorption band (Fig. S1) for the respective complex. Such changes are not uncommon for reagents that are not bound to DNA structure though intercalative mode of binding.^{30,31} Luminescence studies revealed that addition of CT-DNA to the aq. buffer solutions of **1** and **2** led to the enhancement in the fluorescence intensity of the respective complexes. The binding affinity K_a , and site size S for the respective complexes were calculated by fitting the obtained data from UV-Visible and fluorescence spectroscopic titrations into McGhee Von-Hippel model (table 1). The binding parameters evaluated using these two different optical titration methods were found to be in good agreement. The relatively high affinities observed suggest that the interaction of these systems with DNA is not solely due to electrostatics.

Table 1. Binding parameters that were evaluated from UV-Visible and fluorescence titrations for **1** and **2** with CT-DNA.

	1		2	
Titration	K_a [Mol ^{−1}]	S [bp]	K_a [Mol ^{−1}]	S [bp]
Absorbance	3.2×10^5	0.8	5.3×10^5	1.0
Luminescence	1.6×10^5	0.9	2.1×10^5	0.9

Isothermal titration calorimetry studies with CT-DNA.

Binding constants and other thermodynamic parameters for the interaction of complexes **1** and **2** with CT-DNA were also evaluated using isothermal titration calorimetry (ITC) measurements. Relevant thermographs are displayed in figures 2a and 2b. The binding affinity of **1** ($K_a^1 = 1.18 \times 10^5 \text{ M}^{-1}$) and **2** ($K_a^2 = 1.57 \times 10^5 \text{ M}^{-1}$) towards CT-DNA were in good agreement with those obtained from UV-Visible and luminescence titrations. Since, ITC and spectroscopic techniques used two different binding models to calculate the binding constant (K_a) and site size (N), it is not unreasonable to see a minor difference in the values evaluated for K_a and N (bp) following two different techniques. Data are shown in

table 2 clearly reveal that the binding process was entropically driven with the best fit for the integrated heat data being obtained using a single set of identical sites model.

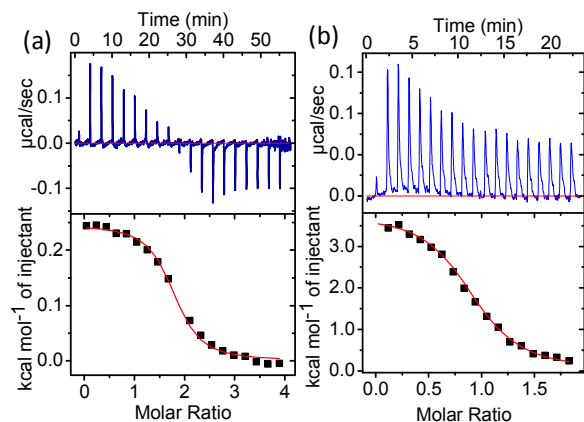


Figure 2. ITC binding profile plots for binding of **1** and **2** with CT-DNA.

This thermodynamic profile is indicative of non-covalent interactions between DNA and the complexes and is consistent with hydrogen bonding. Since both complexes contain amino acid moieties with a set of donor and acceptor sites these observations are not unexpected: we have previously demonstrated that somewhat related systems possessing hydrogen bonding sites can bind DNA with high affinities.³² All these observations suggested that **1** and **2** interact with CT-DNA predominantly through groove binding and certainly not through intercalation. To corroborate this result, we performed the viscosity measurements with CT-DNA which also confirmed the groove binding of complex **1** and **2** (Fig. S2). This is consistent with the observed evidence of hydrogen-bonding, as this interaction would require the amino-acid based ligand to sit in a DNA groove so that it can make close contact with base pairs.

Plasmid DNA photo-cleavage: Gel electrophoresis studies.

We also investigated possible mechanisms of cell death caused by complexes **1** and **2**. To assess the DNA-damaging ability of **1** and **2** upon photo-irradiation, we conducted the gel electrophoresis experiment with pUC19 plasmid DNA after incubation with **1** or **2**. Agarose gel images of pUC19 plasmid DNA (Fig. 3) clearly revealed that the photo-irradiated of plasmid DNA samples incubated with **1** and **2** leads to conversion of supercoiled DNA (SC) into nicked circular form (NC). No such DNA cleavage has been found when the dark incubated samples ran on the agarose gel. It is well documented in the literature that Ru(II)-polypyridyl complexes can convert water or molecular oxygen into the respective ROS species (OH^\bullet or $^1\text{O}_2$) following an energy transfer process involving their $^3\text{MLCT}$ state.^{5,28–31} To understand the role of ROS which could be responsible for the observed pUC19 plasmid DNA cleavage, the control experiments were performed by incubating the plasmid DNA **1** (Fig. 3a) or **2** (Fig. 3b) along with DMSO (a OH^\bullet radical scavenger) or D_2O (which

enhances $^1\text{O}_2$ lifetime) or NaN_3 (an $^1\text{O}_2$ quencher) under the same photo-irradiation conditions. These reaction mixtures were subjected to agarose gel electrophoresis (Lanes 1-5, Fig. 3a for complex **1**; Fig. 3b for

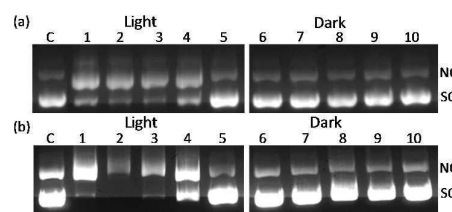


Figure 3. Electrophoresis in agarose gel of pUC19 plasmid DNA with **1** (a) and **2** (b) following photo-irradiation for 4 h (lanes 1–5) and incubation in the dark conditions for 4 h (lane 6–10) in presence of different inhibitors. Lane C: Control plasmid DNA, lane 1: DNA with **1/2** (50 μM), lane 2: DNA with **1/2** (100 μM), lane 3: DNA with **1/2** (100 μM) in presence of D_2O , lane 4: DNA with **1/2** (100 μM) in presence of DMSO, Lane 5: DNA with **1/2** (100 μM) in presence of NaN_3 . For experiments $[\text{DNA}] = 40 \mu\text{g/mL}$, $[\text{NaN}_3] = 100 \text{ mM}$, $[\text{D}_2\text{O}] = 100 \text{ mM}$, $[\text{DMSO}] = 200 \text{ mM}$; Lanes 6–10 represents the samples incubated in dark with same experimental conditions that were followed for lanes 1–5.

complex **2**). Simultaneous control experiments were performed after incubation in the dark under otherwise identical experimental conditions (Lanes 6–10, Fig. 3b for complex **1**, Fig. 3b for complex **2**). It is evident from Fig. 3 that, on incubation with complex **1** or **2** under irradiation, pUC19 plasmid DNA is converted from SC to NC DNA. For experiments that were performed in the presence of D_2O , a distinct increase in the SC to NC (lane 3) forms was observed. For experiments that were performed after incubation with DMSO, the pattern of the damage to the plasmid remained unchanged (lane 4). These observations indicate that the photo-irradiation of **1** or **2** was generated *in-situ* ROS species ($^1\text{O}_2$ and not OH^\bullet). To further confirm this, the samples were co-incubated with NaN_3 , (efficient scavenger for $^1\text{O}_2$, lane 5). It is evident from lane 5 that the presence of NaN_3 results in the inhibition of conversion of SC into NC. Thus, gel electrophoresis results clearly reveal that both **1** and **2** damage plasmid DNA in the presence of light through an *in-situ* generation of $^1\text{O}_2$. Results of the control experiments also confirm that these two complexes fail to generate any DNA damage in the dark. To prove the *in-situ* generation of $^1\text{O}_2$ on photo-irradiation of **1** and **2**, we have recorded its phosphorescence band for $^1\text{O}_2$ that appears in the NIR region at 1275 nm (Fig. S3).

Evaluation of $^1\text{O}_2$ production ability by **1** and **2**.

For PDT application, relatively high quantum yield of $^1\text{O}_2$ (~ 0.5) is desired.¹⁰ We utilized the *N,N*-dimethyl-4-nitrosoaniline (RNO)/imidazole assay for evaluating the relative quantum yield efficiency for $^1\text{O}_2$ generation by complexes **1** and **2** on irradiation with a visible light source having $\lambda \geq 450 \text{ nm}$ (table 2, Fig. S4). Singlet oxygen (produced *in-situ*) reacts with imidazole and leads to the generation of a tetrannular intermediate species, which eventually, quenches the absorption band for RNO at 440 nm either in acetonitrile or water (Fig. S4b, d, g and h). The universal standard, phenalenone was used as the reference for the determination

ARTICLE

of singlet oxygen quantum yield.³⁶ The nature of the solvent had pronounced influence on the efficiency photosensitization and generation of ¹O₂.

Table 2. Singlet oxygen quantum yield for complex **1**, **2** and [Ru(bpy)₂(dmbpy)]²⁺

Complex	Water	Acetonitrile
1	0.20	0.80
2	0.25	0.72
[Ru(bpy) ₂ (dmbpy)] ²⁺	0.32	0.57

Eventually the ¹O₂ quantum yields were calculated using the equation 1 and data for respective complexes are provided in table 2. The measured quantum yield values of these two complexes were found to be comparable for analogous compounds reported in literature.²⁸

$$\Phi_{\text{sample}} = \Phi_{\text{reference}} \frac{S_{\text{sample}}}{S_{\text{reference}}} \frac{I_{\text{reference}}}{I_{\text{sample}}} \quad \text{equation 1.}$$

Light-induced cytotoxicity: MTT assay

Since photoexcited Ru(II)-polypyridyl complexes are known to generate ROS, we then examined the light-induced cytotoxicity of complexes **1** and **2** towards the two different cancer cell lines. Live human lung cancer (A549) and colon cancer (Hct116) cells were incubated with **1** and **2** for 4 h in the dark and photo-irradiation conditions. The cells were photo-irradiation at the MLCT wavelength of **1** and **2** with visible light source ($\lambda_{\text{range}} \sim 450 - 480 \text{ nm}$ having the flux of 10 J/cm^2) under otherwise identical conditions. MTT assay studies revealed (Fig. 4) that these two complexes are non-toxic in dark conditions ($\text{IC}_{50} > 300 \mu\text{M}$) with more than 85 % of the cells surviving even at $300 \mu\text{M}$ concentration. However, upon photo-irradiation, the calculated IC_{50} values were 25 and $28 \mu\text{M}$ respectively for complexes **1** and **2** (table. S1). A substantial difference in light and dark IC_{50} values suggested that these complexes could have possible application as PDT agent.

It is worth mentioning that literature reports suggest most initial drug screening is performed with two-dimensional cell culture.^{9,37–39} A solid cancer, such as those of the breast, colon, stomach, lung and liver, is a tumor mass that is hypoxic at the center and denser than the surrounding tissue. In this context, 3D cell culture model has been developed, where 3D cell culture model performs better than the commonly used 2D models in capturing the complexity of in-vivo processes within the tumor microenvironment and provide a more realistic physiological environment than traditional monolayer cultures.^{37,40} 3D tumor spheroids mimic the pathophysiology of tumors, including hypoxic/necrotic regions as well as mimicking the changes in cell shape, the high proportions of quiescent cells, alterations in gene expression profiles, and diminished permeability to drugs.⁴¹ Spheroids exhibit the phenomena of multicellular resistance (MCR), which is manifested in the diminished efficacy of chemotherapeutics similar to in-vivo activities.⁴² Thus, to examine the cytotoxicity

of these two photo-responsive Ru(II)-polypyridyl complexes towards such 3D tumors under more biologically relevant conditions, treatment efficacy was examined with 3D tumor model by generating tumor spheroids with A549 and Hct116 cells. Spheroids of ca. $600 \mu\text{m}$ in diameter were dosed with compounds **1** and **2** ($10 - 300 \mu\text{M}$) and then these tumors were either kept in the dark for control experiments or were kept

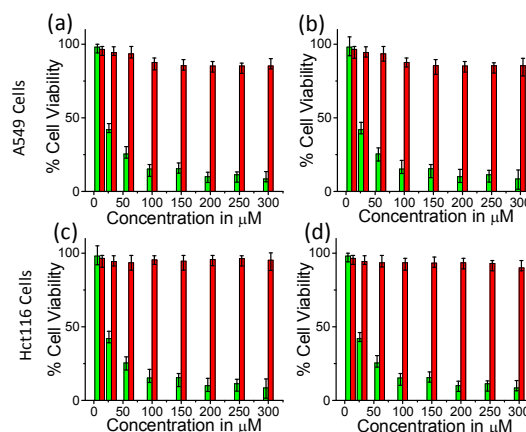


Figure 4. Photo-induced cytotoxicity of **1** (a, c) and **2** (b, d) in 2D tumors of A549 cells (top) and Hct116 (bottom) after photo-irradiation for 4 h (green bars), and in dark for 4 h (red bars).

under photo-irradiation (Fig. S5). Significant photo-induced cytotoxicity was observed for both complexes (**1** and **2**) with an IC_{50} values two different cell lines are provided in the table S2. For control experiments, where cells were kept in the dark conditions, more than 95 % of the cell survival was observed for [**1**] or [**2**] of $\sim 300 \mu\text{M}$. These data clearly revealed that both complexes are non-toxic to live A549 and Hct116 cells when incubated in dark and showed significant light-induced cytotoxicity towards these cells. Further, our studies revealed that, in 3D tumor models a 2-fold increase in IC_{50} values as compared to the 2D cell models. One of the required properties for an ideal photosensitizer is that the PS should have a higher phototoxic index ($\text{PI} = \text{IC}_{50} \text{ in the dark} / \text{IC}_{50} \text{ upon irradiation}$)²⁸ and must be activated at a specific wavelength, preferably in the visible or near-IR region due to the deeper penetration of light into tissue. In this present study, we have also calculated the PI for our photo-active molecules with excitation wavelength at $\lambda = 450 \text{ nm}$. From the table S2, the calculated PI values for the complex **1** and **2** towards A549 cancer cell lines are $> 10 \%$ and $> 4 \%$ in 2D and 3D cell cultures respectively. We also had performed MTT assay studies to find out the specific ROS that could be accounted for the cell death. For this, we incubated cells in the presence of two different ROS scavengers, such as DMSO (OH^\bullet scavenger) and NaN_3 ($^1\text{O}_2$ scavenger) and found that the $^1\text{O}_2$ is the responsible species for the cell death (see supporting information fig. S6). Thus, the observed cell death was due to the *in-situ* (photo-induced) generation of $^1\text{O}_2$ by **1** and **2**.

Single-Cell Gel electrophoresis (SCGE): Comet assay.

To investigate the possibility of DNA damage at cellular level, single-cell gel electrophoresis (SCGE) or comet assay was performed.⁴³ The comet assay is based on the lyses of cells with non-ionic detergent like Triton-X and high-molarity sodium chloride. This treatment removes/dissolves cell membranes, cytoplasm, and nucleoplasm as well as disrupts nucleosomes, as most of the histone is solubilized by alkali solution.⁴⁴ We treated A549 cells with **1** (30 μ M) and **2** (30 μ M) following photo-irradiation. For control experiments, an identical reaction mixture was kept in the dark conditions. From Fig 5a, the electrophoresis of the comet slide containing cells treated with **1** in presence of light reveals cleavage of DNA (Fig. 5a, i-iv); but no cleavage was observed in the case of cells treated with **1** in dark conditions (Fig. 5a, v-viii). Comparable results were observed for complex **2** (Fig. 5b i-iv, Photo-irradiated cells and Fig. 5a v-viii, cells in the dark). Images from fluorescence microscopy revealed the expected comet-like structures and the intensity of the comet tail relative to the head reflected the number of DNA breaks. SYBR green was used to visualize DNA on exposure to UV light. Increases in the longer and darker comet tail directly reflect the extent of DNA damage. The fluorescence intensity profile plots for **1** (Fig. 5a iii, viii) and **2** (Fig. 5b iii, viii) indicate that DNA damage in the tail is higher than the heads of the comets. The percentage of DNA damage was quantified by using ImageJ software (fig. S7). From this data, we conclude that the complex **2** caused more damage to the DNA in A549 cells than the complex **1**. One could find the photo-irradiated samples cleaved cellular DNA more efficiently compared with the dark incubated samples.

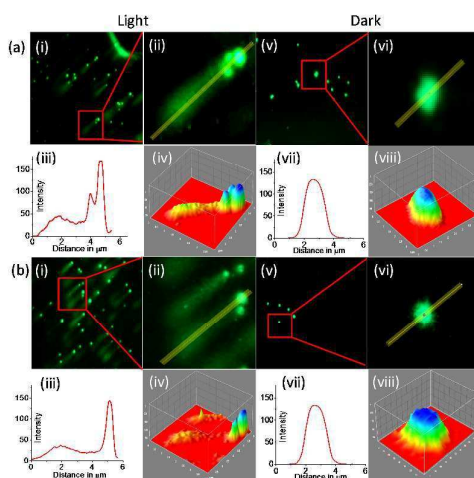


Figure 5. Comet images of A549 cells treated with **1** (a) and **2** (b). CLSM images (i-iv) photo-irradiated and (v-viii) treated in the dark. The DNA damage was visualized using microscope under VU light illumination.

Cellular uptake and CLSM imaging studies.

Since complexes **1** and **2** showed significant photo-induced cytotoxicity towards A549 cancer cell lines, we have further conducted confocal laser scanning microscopy (CLSM) studies to identify the cellular accumulation of these photo-toxic

complexes. The cell imaging studies were performed by incubating **1** (Fig. 6a) and **2** (Fig. 6b) with live A549 cells. Co-localization studies were then performed using commercially available mitotracker green. Figure 6a, b shows that neither of the complexes entered the cell nucleus. A close comparison of the merge image with mitotracker green clearly revealed the intracellular emission of **1** and **2** from the cytoplasm. From the merge images one can see that both the complexes were targeting the mitochondria. Also, a distinct emission was observed from the cell membrane, indicating that the cell membrane is also a target for these reagents. Literature reports have demonstrated that more lipophilic cationic reagents generally accumulate preferentially in the cell membrane while analogous reagents with comparable overall charge but relatively lower lipophilicity preference the nucleus.^{45,46} The dot-like structures with red fluorescence observed from the cytoplasm and cell membrane are reminiscent of another lipophilic Ru(II)-polypyridyl complexes which is observed in phospholipid bilayer of the cell membrane.⁴⁷

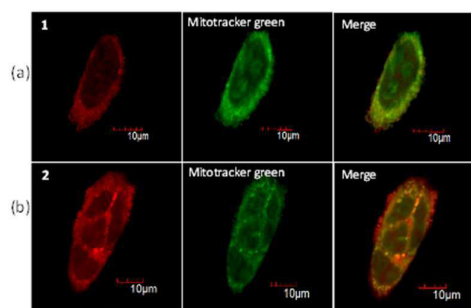


Figure 6. CLSM images of A549 cells incubated with **1**(a) and **2** (b). Co-localization studies performed with mitotracker green.

Such dot like structures, scattered in the cytoplasm, are attributed to localization of these reagents in cytoplasmic vacuoles, which are known to play a subordinate role in endocytosis.^{48,49}

Partition coefficient logP measurement.

The partition coefficient (logP) values were calculated using the shake-flask method to determine the lipophilicity of **1** and **2**. Results shown in table 3 clearly reveal that the lipophilicity of complex **1** (logP = -1.31) is higher than **2** (logP = -1.72). The logP for the model Ru(II)-polypyridyl complex ([Ru(bpy)₂(dmbpy)]²⁺; logP = -1.01) was also evaluated. These values suggest that the conjugation of the amino acids i.e., tyrosine and the tryptophan to the Ru(II)-polypyridyl moiety have certainly influenced the logP values of the final complexes **1** and **2**.

Table 3. Lipophilicity (logP) values obtained for **1**, **2**, and [Ru(bpy)₂(dmbpy)]²⁺ using the shake-flask method.³¹

Complex	1	2	[Ru(bpy) ₂ (dmbpy)] ²⁺
LogP	-1.31 ± 0.02	-1.72 ± 0.05	-1.01 ± 0.04

ARTICLE

Journal Name

It has been previously argued that the lipophilicity of a complex is more important than its overall charge in influencing cellular internalization.^{50–52} The lipophilicity for the complexes used in this study follows the order $[\text{Ru}(\text{bpy})_2(\text{dmbpy})]^{2+} > \mathbf{1} > \mathbf{2}$ (table 5). The trend in cellular internalization expected by these data was confirmed by MP-AES (Microwave Plasma Atomic Emission Spectroscopy) studies (ESI, table S2) as cellular uptake follows the same order i.e., $[\text{Ru}(\text{bpy})_2(\text{dmbpy})]^{2+} > \mathbf{1} > \mathbf{2}$.

Wound Healing assay

As it was discussed above the metastasis of tumors is a multistep biological process that allows cancer cells to get away from the primary tumor, survive and grow in some other parts of the human body.^{11,10,53,54} Many researchers have suggested that effective therapy for cancer or efficient ways of treating a cancer patient essentially depends on the anti-metastatic activity of the chemotherapeutic PS drugs.^{3,10} from the MTT assay, it is evident that these two complexes have good potential for interrupting cancer cell proliferation in the presence of visible light. To further check this possibility, we performed wound healing assay experiments with highly metastatic MDA-MB231 cells. Complexes **1** and **2** were incubated with MDA-MB231 cells in the presence of visible light, while analogous model experiments were performed in the dark conditions. A wound was created using wound creating stick just prior to the addition of the complexes **1** or **2**. Then these MDA-MB231 cells were incubated with **1** or **2** for 4 h on photo-irradiation and then cells were kept in the dark for 10 h. For control experiments, MDA-MB231 cells were incubated with **1** or **2** for 14 h in dark. Bright-field images were captured at different time intervals. However, images recorded at 0 min and after 10 h are shown in fig. 7. fig. 7d (for complex **1**) and fig. 7h (for complex **2**) clearly reveal that cells that were initially irradiated for 4 h with visible light in the presence of **1** or **2**, failed to migrate and to heal the wound.

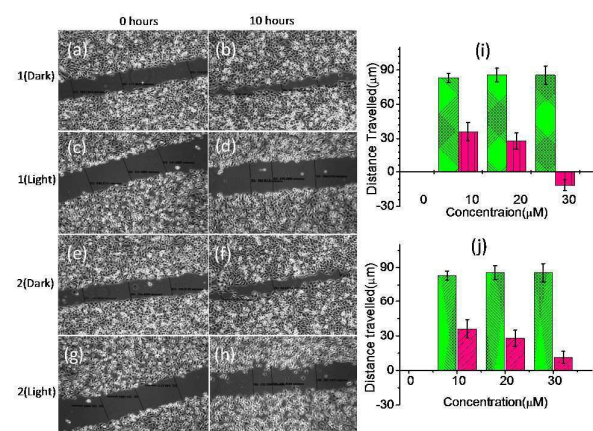


Figure 7. MDA-MB231 cells incubated with compound **1**(a-d) and **2**(e-h) at 0 h and 10 h. The graphical representation of the distance travelled by cells in the presence of **1** (i) and **2** (j) in the presence and absence of light. To further investigate this possibility an invasion assay was undertaken.

However, figs. 7b (for complex **1**) and 7f (for complex **2**) reveal that MDA-MB231 cells that were kept in dark with complexes **1** or **2** could migrate to the other end and the respective wound was almost healed. The distance travelled by the cells were calculated and plotted as a function of the concentration of reagent **1** (fig. 7i) or **2** (fig. 7j). These results indicate that the two Ru(II)-polypyridyl complexes do inhibit cell migration suggesting they may possess anti-metastatic activity.

Invasion assay.

As was discussed above one of the hallmarks of cancers is cell invasions and metastasis into nearby and distal organs initiated by various protein de-regulations of PTEN, MMPs, EGFR, and CD44. Highly metastatic cells lose cell to cell adherence and break off. These invade basement membrane and endothelial walls for entering the blood stream or lymph nodes. These cells are then carried away to distal organs are deposited and result in primary metastasis.

Here, the cells again invade endothelial walls and basement membrane, gets deposited, undergo cell division, and grow to form tumors. The tumor-forming cells still possess the characteristics to invade and settle into other organs for tumor formation. This eventually results in a secondary metastasis. Therefore, invasion and metastasis are two important aspects that need to be controlled to prevent spreading of cancer throughout the human body. To assess the potential of **1** and **2**

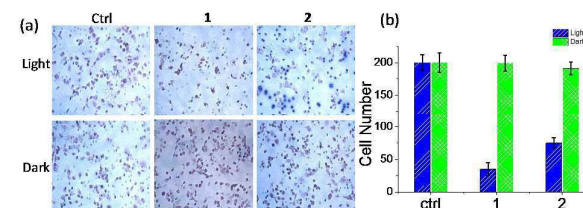


Figure 8. (a) Effect of **1** and **2** on MDA-MB231 cell invasion, (b) The percentage of cells invaded was reduced to 17.5% with **1** and 37.5 % with **2** in the presence of light (blue bars). However, there was no change in the dark controls (green bars).

in controlling cell invasion, we incubated complex treated highly metastatic live MDA-MB231 cells on top of matrigel and allowed the cell to invade in the absence (control experiment) and presence of visible light. The percentage of cells invaded was then calculated using the equation 2.

$$\% \text{ Invasion} = \frac{\text{mean number of cells invading through Corning Matrix coated permeable support membrane}}{\text{number of cells migrating through uncoated permeable support membrane}} \times 100 \text{ mean}$$

equation 2.

Relative to 100 % cells invasion for a control experiment, the percentage of cells that invaded through matrigel was significantly reduced when experiments were performed with **1** (17.5 %) and **2** (37.5 %) under light irradiation conditions (fig. 8). This experiment also revealed that the complex **1** prevents cell invasion more efficiently than complex **2**.

Complex **1** and **2** induces apoptosis by caspase-3 activation.

We next set out to elucidate the molecular mechanism responsible for light induced cell death by complexes **1** or **2**. We examined if light induced cell cycle arrest occurred through the activation of DNA damage signalling pathways. For this, A549 cells were treated with complex **1** or **2** in the dark or under light irradiation. It was found that there was a significant increase in the expression level of apoptosis marker caspase-3 in photo-irradiated cells (fig. 9).

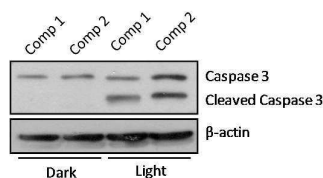


Figure 9. A549 cells growing in serum-containing medium were treated with **1** and **2** for 24 h prior to lysate preparation and immunoblotting with antibodies. The blot was probed with primary antibodies against caspase-3. β -Actin levels were used as a loading control. All results are representative of two independent experiments.

Whereas in the dark treated samples there was no difference in the expression level of caspase-3. This indicates that on irradiation complex **1** and **2** induce apoptosis in the A549 cells. As discussed earlier, exposure to visible light for cells incubated with **1** or **2** resulted in the generation of ROS (1O_2). Singlet oxygen is known to damage the DNA and is also responsible for altering the mitochondrial trans membrane potential. Literature reports reveal that the pro-apoptotic proteins, released from mitochondria, are responsible for activation of caspase-3 and the cell finally leads to apoptosis. Thus, these photoactive compounds could be used for the treatment of solid tumors by specifically illuminating in the visible light which would not cause any ROS production in the dark condition.

4. Experimental

Materials and methods.

All chemicals were purchased from Sigma-Aldrich unless otherwise indicated. 1H NMR spectra were recorded on a Bruker FT-NMR spectrometer at room temperature. ESI-MS measurements were carried out on a Waters QToF-Micro instrument. UV-Vis spectra were obtained by using a Cary 500 scan UV-Vis spectrometer. Complexes **1** and **2** were converted into their water-soluble chloride salts via anion metathesis. The CT-DNA concentration per nucleotide was determined by absorption spectroscopy by using the molar absorption coefficient ($6600 \text{ mol}^{-1} \text{ dm}^3 \text{ cm}^{-1}$) at 260 nm. The emission spectra were obtained using Edinburgh instrument Xe-900 spectrofluorometer. Confocal microscopy images acquired using Olympus Fluoview microscope. Partition coefficient (logP) measurements were calculated using the shake-flask (n-octanol/water) method. The absorbance of the respective complex in each phase was determined using UV-Vis spectroscopy. ITC experiments were performed with the

Microcal iTC200. CT-DNA concentration (0.1 mmol) and complexes **1** (5 mmol), **2** (5 mmol) concentrations were used for these experiments. All titrations were conducted in Tris-HCl buffer (5 mmol Tris and 25 mmol NaCl), pH = 7.4 at 25 °C. The resulting isotherms were fitted with the one set of site binding model provided with Microcal iTC200. A549 and Hct116 cells were cultured in DMEM respectively supplemented with 10% FBS and penicillin/streptomycin. Cell lines were maintained at 37 °C in an atmosphere of 5 % CO_2 and routinely sub-cultured. Cytotoxicity tests were performed using MTT assay in triplicate.

Synthesis of Complexes **1** and **2**: Complexes **1** and **2** were synthesized following previously reported literature procedures. The chloride salts of **1** and **2** were obtained by anion metathesis of their respective PF_6^- salts using $[nBu_4N]Cl$ in acetone for improved water-solubility. Characterization data for respective complex are given below.

Characterization of complex 1 (PF_6)₂: Yield: 58.3 % (196 mg, 0.17 mmol); 1H NMR (CD_3CN , 500 MHz): δ 8.73 (s), 8.53 (d, J = 8.4 Hz), 8.09 (t, J = 7.9 Hz), 7.88 (dd, J = 5.8, 2.6 Hz), 7.78-7.70 (m), 7.64 (d, J = 7.9 Hz), 7.62-7.59 (m), 7.58 (d, J = 5.8 Hz), 7.43 (t, J = 6.7 Hz), 7.31 (d, J = 5.5 Hz), 7.13 (dd, J = 8.5, 3.5 Hz), 6.75 (dd, J = 8.5, 4.5 Hz), 4.86-4.80 (m), 4.18 (q, J = 8.5 Hz), 3.22 (dd, J = 14.0, 5.8 Hz), 3.09 (dd, J = 14.1, 8.6 Hz), 2.59 (s), 1.24 (t, J = 7.1 Hz). ESI-HRMS (m/z) for formula: $C_{43}H_{39}F_6N_7O_4PRu$; calculated 964.1743; found: 964.1740.

Characterization of complex 2 (PF_6)₂: Yield: 50 % (180 mg, 0.159 mmol). 1HNMR (CD_3CN , 200 MHz): δ ppm 9.19 (d, J = 1.2 Hz), 8.60 (s), 8.49 (d, J = 8.1 Hz), 8.38 (s), 8.06 (dd, J = 11.1, 4.6 Hz), 7.81 (d, J = 5.7 Hz), 7.70 (d, J = 5.0 Hz), 7.57 (d, J = 5.9 Hz), 7.52 (s), 7.39 (t, J = 6.5 Hz), 7.25 (s), 7.21 (d, J = 4.3 Hz), 7.17 (s), 7.03 - 6.89 (m), 5.03 - 4.88 (m), 4.15 (q, J = 7.1 Hz), 3.46 - 3.34 (m), 2.55 (s), 1.21 (t, J = 7.1 Hz). ESI-HRMS m/z (%) for formula $C_{45}H_{40}N_8O_3Ru$, calculated 841.2183; found: 841.2184.

DNA binding titrations.

For absorption titrations, complexes **1** and **2** were converted to their chloride salts by treatment with $[nBu_4N]Cl$ in acetone. Complex solution (10 mL of a 10 mmol stock) in Tris-HCl buffer was then diluted into Tris buffer to give a final concentration of about 5 mm Tris buffer. This was loaded into another identical cuvette and placed in the reference cell of the spectrometer. After 30 min cell equilibration, the first spectrum was recorded between 600-200 nm. DNA solution (2-5 mL) was then added to both the sample and reference cell and mixed. The spectrum was taken again, this time showing the hypochromic shift indicating the formation of a drug-DNA complex. The titration process was repeated until there was no change in the spectrum for at least four titrations, indicating binding saturation had been achieved. Both buffer and complex solutions showed insignificant emission, so no reference cell was used. Buffer (3 mL) was loaded in a 1 cm path-length luminescence cuvette; an aliquot of buffer was removed and replaced with the same volume of a stock solution of complex (final concentration 5 mm). The cuvette was loaded into the spectrophotometer and incubated at 25 °C. After equilibration, the emission spectrum of the solution

ARTICLE

Journal Name

was recorded by using the excitation wavelength characteristic of the complex. A concentrated stock of CT-DNA solution (2 mL) was added to the cuvette and mixed, and then the emission spectrum was recorded, which showed an enhancement in emission. This procedure was continued until the emission became constant. Emission titrations were successfully fitted to the McGhee–von Hippel model for binding to an isotropic lattice.

Isothermal Titration Calorimetry (ITC) studies.

ITC experiments were performed with the Microcal iTC200. CT-DNA concentration (0.1 mmol) and complexes **1** (5 mmol), and **2** (5 mmol) concentrations were used for these experiments. All titrations were conducted in Tris-HCl buffer (5 mmol Tris and 25 mmol NaCl), pH = 7.4 at 25 °C. In each titration, CT-DNA was loaded into the cell and complexes **1** or **2** were taken into the syringe. Aliquot of 2 µL of complexes were added to the cell containing DNA. In each experiment, the raw isotherms were corrected for the heat of dilution by subtracting the isotherms representing the complexes injected into the Tris-HCl buffer. The resulting isotherms were fitted with the one set of site binding model provided with Microcal iTC200.

Singlet oxygen measurement studies.

N,N-Dimethyl-4-nitrosoaniline/histidine assay.

The singlet oxygen production was measured by the N,N-dimethyl-4-nitroso- aniline/histidine assay based on the oxidation of histidine by singlet oxygen and the subsequent reaction of the oxidised histidine with N,N-dimethyl-4-nitrosoaniline as previously described.^{45,68} The absorbance of the compound was adjusted to approximately 0.2 at the irradiation wavelength. In practice, 20 mM DMSO stock solution of the compound to measure were diluted in 4 mL PBS solution (pH 7.4) containing N,N-dimethyl-4-nitrosoaniline (25 µM) and histidine (0.01 M) and irradiated in fluorescence quartz cuvettes (width 1 cm). Bleaching of N,N-dimethyl-4-nitrosoaniline was followed by monitoring of the absorption at 440 nm. Negative control experiments were run by repeating the measurements in the absence of histidine. The same conditions were also used for singlet oxygen detection in acetonitrile, except that imidazole was used instead of histidine due to the low solubility of histidine in this solvent. In addition, the absorbance peak of N,N-dimethyl-4-nitrosoaniline shifts to 415 nm in acetonitrile. The absorbance at 440/415 nm was then plotted as a function of irradiation time and the quantum yields of singlet oxygen formation (Φ_{sample}) were calculated using phenalenone as the standard ($\Phi_{\text{reference}}$) with the following formula:

MTT assay and CLSM studies.

Cell cultures were treated with 0-300 µM solutions of **1** and **2** in triplicate for 24 h. After incubation 5 µL of MTT reagent was added and incubated for 4 h. MTT = (3-(4, 5-dimethylthiazol-2-yl)-2,5-diphenyltetrazolium bromide) dissolved in serum-free media. The media was removed and the formazan dissolved using isopropanol and the absorbance at 570 nm quantified by the plate reader (reference 620 nm). IC₅₀ values for the two

complexes were found to be >300 µM. A549 cells were cultured in DMEM media. Cell lines were maintained at 37° C in an atmosphere of 5 % CO₂ and routinely sub-cultured. For CLSM, cell cultures were grown on 6 well plate with coverslips, after 24 h of incubation the cells were treated with solutions of **1** and **2** (30 µM,) in serum containing media and incubated for 4 h. After incubation media was removed and cells were washed with 1XPBS buffer. Co-localization staining studies were performed using mitotracker green form life technologies. Cells were fluorescently imaged on a Fluoview confocal laser scanning microscope by using 60X oil-immersion lenses. Complexes **1** and **2** were excited with a laser at 442 nm and emission monitored at 620 nm (red) wavelengths. Mitotracker was excited at 490 nm.

Wound healing (scratch motility) assay.

MDA-MB-231 cells were cultured in Leibowitz's L15 medium with 10 % FBS. 1 X 10⁵/mL cells were seeded in 6 well plate and incubated for 24 h at 37 °C, 5 % CO₂ incubator to form a monolayer. After 24 h gaps were created using pipette tip on the confluent monolayer and washed with media to remove cellular debris. The fresh medium supplemented with 10 % FBS was added into well and incubated with **1** and **2** (30 µM) for 4 h to allow the uptake by cells. Following with same conditions one cell culture plate was photo-irradiated for 4 h and the other place kept in the dark conditions. The cell migration observed and imaged at regular intervals (0- 10 h) using Nikon live cell imaging microscope for 10 h. The rate of migration of the cells was calculated using image pro 6.0 software provided along with Nikon microscope.

Comet assay.

Live A549 cells were incubated with **1** and **2** for 4 h and suspended the cells into PBS buffer. This suspension of the cells was embedded into the low melting agarose (0.5 %) gel. 100 µL of this mixture is poured on top of the agarose pre-coated comet slides. The coverslip was placed on top of the comet slides and removed after solidification of agarose. A549 cells were lysed with an alkaline solution over night at 4° C. Then slides were removed and rinsed twice with the rinsing solution to remove the residual amounts of excess salt and detergents. The comet slide incubated for 2 h in electrophoresis unit in 1X PBS buffer solution. Voltage (0.6 V/cm for 25 min with current of 40 mA) applied to accumulate the damaged DNA at the end of the cathode. Then slide was removed from electrophoresis chamber and rinsed with 400 mL of distilled water. Then the comet slide was placed in staining solution (syber green solution) for 20 min. Again, the comet slide was rinsed with 400 mL of deionized water to remove the excess stain. The DNA damage was visualized using microscope under VU light.

Viscosity measurements.

Viscosity studies were done in a Cannon-Manning semi micro viscometer (size 50) immersed in a thermostat bath maintained at 27 ± 1° C. The concentration of CT-DNA was kept constant at 1 mmol and viscosity of the CT-DNA was measured by increasing the concentration of the

ethedumbromide, **1**, **2** and $[\text{Ru}(\text{bpy})_3]^{2+}$. The flow times were measured after thermal equilibration of at least 30 min. Each sample was measured three times and the averaged time was used in calculations.

Invasion assay.

2.5×10^4 MDA-MB231 highly metastatic breast cancer cells seeded onto each well of 24 well matrigel plate chamber. Below the matrigel chamber 750 μL of fetal bovine serum was placed as chemo-attractant for the MDA-MB231 cells to invade. Cells were treated with complex **1** and **2** for 4 h and then either exposed to dark or visible light conditions for 4 h. The cells were then allowed to invade the matrigel over-night at 37 °C in a humidified 95 % incubator. Next day, the non-invading cells were removed using moistened cotton swabs. Cells were fixed with 100 % chilled methanol for 15 min and then washed with phosphate buffered saline (1 X PBS) three times. 0.4 % crystal violet was prepared and then 500 μL was applied into the chamber containing matrigel and invaded cells. After 15 min of crystal violet staining, three PBS washes given and then air dried. The chamber was then placed under an inverted microscope to count the number of invaded cells.

Western blotting.

Cells were lysed in TNN buffer (50 mM Tris, pH 7.5, 5mM EDTA, 0.5 % NP40 150 mM NaCl and 1 mM DTT), supplemented with protease inhibitor cocktail. The concentration of total protein in the cell lysate was determined by Bradford reagent (Thermo scientific). 40 μg of each protein was loaded onto 10 % SDS-PAGE, and protein was transferred onto PVDF membrane (Millipore) using western blot technique. After the completion of protein transfer, the membrane was blocked for 2 h at room temperature in 5 % BSA (MP Biomedicals). The blot was then washed with 1 X TBST (Tris buffer saline, 0.1 % Tween 20) 3 times, each for 5 min. The blot was probed with primary antibodies against caspase-3 and β -actin (Santa Cruz) for 2 h in 1:1000 dilutions for caspase-3 and 1:4000 dilutions for β -actin. After washing the blot in 1 X TBST, secondary antibody which is conjugated with Horseradish peroxidase was then added in 1:4000 dilutions in 1 X TBST buffer. The blot was then developed using autoradiography in X-ray film.

Conclusions

Two Ru(II)-polypyridyl complexes conjugated with amino acids tyrosine (**1**) and tryptophan (**2**) were investigated for their potential application as photodynamic therapeutic (PDT) agents. Complexes **1** and **2** showed preferential binding CT-DNA with moderately strong binding affinity $K_a = 1-5 \times 10^5 \text{ mol}^{-1}$. Isothermal titration calorimetry (ITC) studies indicate that the reactions of both **1** and **2** with CT-DNA were entropically driven. Viscosity studies proved that **1** and **2** binds CT-DNA through groove binding. Most importantly, complexes **1** and **2** exhibits photo-induced cytotoxic activity in the presence of visible light at lesser exposure time and found to be low-toxic in the dark conditions (the key feature required by the PDT agents). These two-visible light excitable Ru(II) complexes

showed apoptosis activity, prevents the cells from invasion and capable of producing significant levels of $^1\text{O}_2$ that is which damages the DNA upon photo-irradiation.

Acknowledgements

AD acknowledges SERB (SB/S1/IC-23/2013) and CSIR-Network project (CSC 0134) for financial support. VR and SA acknowledge BRNS and CSIR, respectively, for their fellowships. JAT and MW are grateful for financial support through a Leverhulme Foundation Project grant (RPG-2014-041).

Notes and references

- Z. Huang, *Technol. Cancer Res. Treat.*, 2005, **4**, 283–293.
- C. Mari, V. Pierroz, S. Ferrari and G. Gasser, *Chem. Sci.*, 2015, **6**, 2660–2686.
- M. Ethirajan, Y. Chen, P. Joshi and R. K. Pandey, *Chem. Soc. Rev.*, 2011, **40**, 340–62.
- R. Lincoln, L. Kohler, S. Monro, H. Yin, M. Stephenson, R. Zong, A. Chouai, C. Dorsey, R. Hennigar, R. P. Thummel and S. A. McFarland, *J. Am. Chem. Soc.*, 2013, **135**, 17161–17175.
- M. Ethirajan, Y. Chen, P. Joshi and R. K. Pandey, *Chem. Soc. Rev.*, 2011, **40**, 340–362.
- Z. Huang, *Technol. Cancer Res. Treat.*, 2005, **4**, 283–293.
- A. D. Ostrowski and P. C. Ford, *Dalt. Trans.*, 2009, **48**, 10660–10669.
- W. Cao, W. Zheng and T. Chen, *Sci. Rep.*, 2015, **5**, 9157.
- J. Liu, Y. Chen, G. Li, P. Zhang, C. Jin, L. Zeng, L. Ji and H. Chao, *Biomaterials*, 2015, **56**, 140–153.
- M. R. Gill, S. N. Harun, S. Halder, R. A. Boghazian, K. Ramadan, H. Ahmad and K. A. Vallis, *Sci. Rep.*, 2016, **6**, 31973.
- M. Liu, Z. J. Lim, Y. Y. Gwee, A. Levina and P. a. Lay, *Angew. Chemie - Int. Ed.*, 2010, **49**, 1661–1664.
- V. Ramu, F. Ali, N. Taye, B. Garai, A. Alam, S. Chattopadhyay and A. Das, *J. Mater. Chem. B*, 2015, **3**, 7177–7185.
- B. Dong, X. Song, X. Kong, C. Wang, N. Zhang and W. Lin, *J. Mater. Chem. B*, 2017, **5**, 988–995.
- V. Fernández-Moreira, F. L. Thorp-Greenwood and M. P. Coogan, *Chem. Commun.*, 2010, **46**, 186–202.
- D.-L. Ma, H.-J. Zhong, W.-C. Fu, D. S.-H. Chan, H.-Y. Kwan, W.-F. Fong, L.-H. Chung, C.-Y. Wong and C.-H. Leung, *PLoS One*, 2013, **8**, 55751.
- M. Dickerson, Y. Sun, B. Howerton and E. C. Glazer, *Inorg. Chem.*, 2014, **53**, 10370–10377.
- R. G. Balasingham, M. P. Coogan and F. L. Thorp-Greenwood, *Dalt. Trans.*, 2011, **40**, 11663–74.
- M. Sjödin, S. Styring, H. Wolpher, Y. Xu, L. Sun and L. Hammarström, *J. Am. Chem. Soc.*, 2005, **127**, 3855–3863.
- M. Sjödin, S. Styring, B. Åkermark, L. Sun and L. Hammarström, *J. Am. Chem. Soc.*, 2000, **122**, 3932–3936.
- D. R. Robinson, Y.-M. Wu and S.-F. Lin, *Oncogene*, 2000, **19**,

ARTICLE

Journal Name

- 5548–5557.
- 21 R. Ghanem, Y. Xu, J. Pan, T. Hoffmann, J. Andersson, T. Polívka, T. Pascher, S. Styring, L. Sun and V. Sundström, *Inorg. Chem.*, 2002, **41**, 6258–6266.
- 22 N. R. Smalheiser, W. Zhou and V. I. Torvik, *J. Biomed. Discov. Collab.*, 2008, **3**, 1–10.
- 23 Z.-Z. Li, Y.-L. Niu, H.-Y. Zhou, H.-Y. Chao and B.-H. Ye, *Inorg. Chem.*, 2013, **52**, 10087–95.
- 24 J. D. Knoll, B. A. Albani and C. Turro, *Acc. Chem. Res.*, 2015, **48**, 2280–2287.
- 25 M. A. Sgambellone, A. David, R. N. Garner, K. R. Dunbar and C. Turro, *J. Am. Chem. Soc.*, 2013, **135**, 11274–11282.
- 26 B. Peña, A. David, C. Pavani, M. S. Baptista, J. P. Pellois, C. Turro and K. R. Dunbar, *Organometallics*, 2014, **33**, 1100–1103.
- 27 A. A. Holder, P. Taylor, A. R. Magnusen, E. T. Moffett, K. Meyer, Y. Hong, S. E. Ramsdale, M. Gordon, J. Stubbs, L. A. Seymour, D. Acharya, R. T. Weber, P. F. Smith, G. C. Dismukes, P. Ji, L. Menocal, F. Bai, J. L. Williams, D. M. Cropek and W. L. Jarrett, *Dalton Trans.*, 2013, **42**, 11881–11899.
- 28 C. Mari, V. Pierroz, R. Rubbiani, M. Patra, J. Hess, B. Spingler, L. Oehninger, J. Schur, I. Ott, L. Salassa, S. Ferrari and G. Gasser, *Chem.-Eur. J.*, 2014, **20**, 14421–14436.
- 29 A. K. Renfrew, *Metallomics*, 2014, **6**, 1324–1335.
- 30 A. Ghosh, P. Das, M. R. Gill, P. Kar, M. G. Walker, J. A. Thomas and A. Das, *Chem.-Eur. J.*, 2011, **17**, 2089–2098.
- 31 V. Ramu, M. R. Gill, P. J. Jarman, D. Turton, J. A. Thomas, A. Das and C. Smythe, *Chem.-Eur. J.*, 2015, **21**, 9185–9197.
- 32 V. Ramu, F. Ali, N. Taye, B. Garai, A. Alam, S. Chattopadhyay and A. Das, *J. Mater. Chem. B*, 2015, **3**, 7177–7185.
- 33 M. Stephenson, C. Reichardt, M. Pinto, M. Wa, T. Sainuddin, G. Shi, H. Yin, S. Monro, E. Sampson, B. Dietzek and S. A. McFarland, *J. Phys. Chem. A*, 2014, **118**, 10507–10521.
- 34 H. Yin, M. Stephenson, J. Gibson, E. Sampson, G. Shi, T. Sainuddin, S. Monro and S. A. McFarland, *Inorg. Chem.*, 2014, **53**, 4548–4559.
- 35 T. Gianferrara, A. Bergamo, I. Bratsos, B. Milani, C. Spagnul, G. Sava and E. Alessio, *J. Med. Chem.*, 2010, **53**, 4678–4690.
- 36 R. Schmidt, C. Tanielian, R. Dunsbach and C. Wolff, *J. Photochem. Photobiol. A Chem.*, 1994, **79**, 11–17.
- 37 K. M. Yamada and E. Cukierman, *Cell*, 2007, **130**, 601–610.
- 38 P. Xie, D. S. Williams, G. E. Atilla-Gokcumen, L. Milk, M. Xiao, K. S. M. Smalley, M. Herlyn, E. Meggers and R. Marmorstein, *ACS Chem. Biol.*, 2008, **3**, 305–316.
- 39 A. Kastl, S. Dieckmann, K. Wähler, T. Völker, L. Kastl, A. L. Merkel, A. Vultur, B. Shannan, K. Harms, M. Ocker, W. J. Parak, M. Herlyn and E. Meggers, *ChemMedChem*, 2013, **8**, 924–927.
- 40 S. M. Ehsan, K. M. Welch-Reardon, M. L. Waterman, C. C. W. Hughes and S. C. George, *Integr. Biol.*, 2014, **6**, 603–610.
- 41 A. Abbott, *Nature*, 2003, **424**, 870–872.
- 42 J. D. Knoll, B. A. Albani and C. Turro, *Acc. Chem. Res.*, 2015, **48**, 2280–2287.
- A. R. Collins, *Mol. Biotechnol.*, 2004, **26**, 249–261.
- A. P. De Lima, F. De Castro Pereira, C. A. S. T. Vilanova-Costa, A. De Santana Braga Barbosa Ribeiro, L. A. Pavanin, W. B. Dos Santos and E. De Paula Silveira-Lacerda, *J. Biosci.*, 2010, **35**, 371–378.
- E. Baggaley, M. R. Gill, N. H. Green, D. Turton, I. V. Sazanovich, S. W. Botchway, C. Smythe, J. W. Haycock, J. A. Weinstein and J. A. Thomas, *Angew. Chemie - Int. Ed.*, 2014, **53**, 3367–3371.
- M. R. Gill, J. Garcia-Lara, S. J. Foster, C. Smythe, G. Battaglia and J. A. Thomas, *Nat. Chem.*, 2009, **1**, 662–667.
- N. Zhang, Y. Yin, S. J. Xu and W. S. Chen, *Molecules*, 2008, **13**, 1551–1569.
- O. Zava, S. M. Zakeeruddin, C. Danelon, H. Vogel, M. Grätzel and P. J. Dyson, *ChemBioChem*, 2009, **10**, 1796–1800.
- F. R. Svensson, M. Matson, M. Li and P. Lincoln, *Biophys. Chem.*, 2010, **149**, 102–106.
- E. Ferri, D. Donghi, M. Panigati, G. Prencipe, L. D'Alfonso, I. Zanoni, C. Baldoli, S. Maiorana, G. D'Alfonso and E. Licandro, *Chem. Commun.*, 2010, **46**, 6255–6257.
- G.-L. Law, C. Man, D. Parker and J. W. Walton, *Chem. Commun.*, 2010, **46**, 2391–2393.
- C. P. Montgomery, B. S. Murray, E. J. New, R. Pal and D. Parker, *Acc. Chem. Res.*, 2009, **42**, 925–937.
- Y. Li, Z. Lin, M. Zhao, T. Xu, C. Wang, H. Xia, H. Wang and B. Zhu, *Int. J. Nanomedicine*, 2016, **11**, 3065–3076.
- E. Sahai, *Curr. Opin. Genet. Dev.*, 2005, **15**, 87–96.

Table of Contents Graphic (TOC):

Photo-Induced Cytotoxicity and Anti-Metastatic Activity of Ruthenium(II)-Polypyridyl Complexes Functionalized with Tyrosine or Tryptophan

Vadde Ramu, Sunil Aute, Nandaraj Taye, Rweetuparna Guha, Michael G. Walker, Devaraj G. Mogare^b Jim A Thomas Samit Chattopadhyay and Amitava Das

